Nguyen et al., *BioImpacts.* 2026;16:33591
doi:10.34172/bi.33591
https://bi.tbzmed.ac.ir/

Combined adipose- and umbilical cord-derived extracellular vesicles modulate inflammatory and chondrogenic signaling to promote cartilage repair

Phat Thuan Nguyen[1,2], **Phuc Van Pham**[1,2], **Ngoc Bich Vu**[3,1,2*]

[1]Stem Cell Institute, University of Science, Ho Chi Minh City, Vietnam
[2]Vietnam National University, Ho Chi Minh City, Vietnam
[3]Faculty of Biology-Biotechnology, University of Science, Ho Chi Minh City, Vietnam

Article Info

Article Type:
Original Article

Article History:
Received: 23 Feb. 2026
Revised: 7 May 2026
Accepted: 12 May 2026
ePublished: 7 Jul. 2026

Keywords:
Adipose-derived mesenchymal stem cells,
Umbilical cord-derived mesenchymal stem cells,
Extracellular vesicles,
Exosomes,
Cartilage regeneration,
Medial femoral condyle defect

Abstract

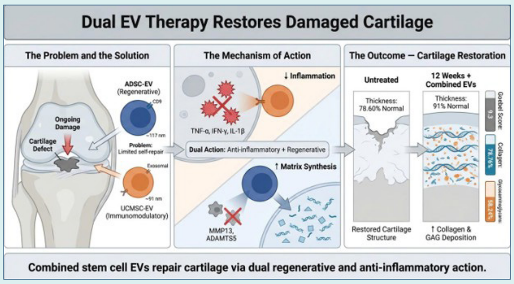

Introduction: Articular cartilage has a limited intrinsic capacity for regeneration following injury, particularly in cases of severe defects. Exosome-based therapy has emerged as a promising cell-free regenerative strategy, with increasing preclinical evidence supporting its therapeutic potential in cartilage repair. As previous studies have indicated that human adipose-derived mesenchymal stem cells (hADSCs) secrete regenerative factors, whereas human umbilical cord–derived mesenchymal stem cells (hUCMSCs) exert immunomodulatory effects, the combined use of exosomes from these two sources may have complementary therapeutic benefits.

Methods: In this study, exosome-enriched extracellular vesicles (EVs) isolated from hADSCs and hUCMSCs were combined, characterized, and evaluated in a cartilage defect model. The isolated EVs displayed a characteristic cup-shaped morphology under transmission electron microscopy, a size distribution ranging from 30 to 200 nm, and high expression levels of the exosomal markers CD9, CD63, and CD81.

Results: Treatment with the combined EVs formulation promoted the regeneration of medial femoral condyle defects at 12 weeks post-injury compared to untreated controls, as demonstrated by an improved macroscopic appearance and scoring, radiographic evaluation, and increased deposition of total collagen, glycosaminoglycans, and aggrecan.

Conclusion: The findings provide proof-of-concept evidence that a combined hADSC- and hUCMSC-derived EVs formulation represents a feasible cell-free approach to cartilage repair.

Introduction

Focal lesions of articular cartilage are frequently encountered in the knee joint. Such lesions constitute a major clinical challenge with considerable socioeconomic implications.[1] These lesions frequently arise from non-contact trauma, which accounts for nearly 32-58% of cases, and are associated with routine daily (45%) and sports-related activities (46%).[2,3] Among the various anatomical locations, lesions of the femoral condyle are the most frequently observed symptomatic chondral defects, followed by defects in the tibial plateau and patellofemoral compartments.[2] If left untreated or inadequately managed, articular cartilage damage may progress to degenerative joint diseases, including osteoarthritis, leading to chronic pain, functional impairment, and a reduced quality of life.[4]

Articular cartilage is difficult to repair due to its avascular, aneural, and alymphatic nature that severely limits its intrinsic capacity for self-repair following injury.[4,5] The management of cartilage-related disorders, including osteoarthritis (OA) and osteochondral defects (OCD), remains one of the most challenging problems in orthopedic medicine.[4,5] Due to the limitations of current treatment strategies, regenerative medicine has emerged as a rapidly evolving field, providing promising therapeutic alternative treatments for OA and OCD.[4-6] Unlike traditional approaches that primarily address

---

*Corresponding author: Ngoc Bich Vu, Emails: vbngoc@hcmus.edu.vn, ngocvu@sci.edu.vn

Research Highlights

What is the current knowledge?

- Articular cartilage has limited intrinsic regenerative capacity, and untreated focal defects often progress toward degenerative joint disease, particularly in younger and active individuals.
- Mesenchymal stem cell (MSC)-derived EVs have emerged as promising cell-free therapeutic agents due to their immunomodulatory and regenerative properties in cartilage repair.
- EVs derived from ADSC (ADSC-EVs) are primarily associated with regenerative and anabolic effects, whereas UCMSC-derived EVs (UCMSC-EVs) are known for their immunomodulatory functions; however, the therapeutic potential of combining these two EV sources has not been systematically investigated.

What is new here?

- A combined formulation of ADSC-EVs and UCMSC-EVs significantly enhanced cartilage repair in a rat medial femoral condyle defect model compared to controls.
- Combined EV treatment modulated early inflammatory signaling and suppressed catabolic gene expression while supporting balanced chondrogenic regulation.
- Histological and molecular analyses demonstrated enhanced deposition of extracellular matrix components, including collagen and aggrecan, indicating that the combined EV strategy promotes structured and sustained cartilage regeneration rather than simple defect filling.

clinical symptoms, regenerative strategies aim to restore the structure and function of damaged cartilage and osteochondral tissue by harnessing biological repair mechanisms.[5] Among these approaches, mesenchymal stem cell-derived exosomes (MSC-Exos) have gained increasing attention as a promising cell-free therapeutic strategy for cartilage regeneration.[6,7] These nanosized intraluminal vesicles, generated within multivesicular bodies and released into the extracellular environment upon fusion with the plasma membrane, play a pivotal role in intercellular communication.[8] Exosomes transfer a diverse cargo of bioactive molecules, including proteins, lipids, messenger RNAs, and microRNAs, thereby influencing the behavior of recipient cells.[9] Preclinical studies have demonstrated the therapeutic efficacy of MSC-Exos in a wide range of disease models, including osteoarthritis.[10] In the context of cartilage repair, exosomes have been shown to promote chondrocyte proliferation, extracellular matrix deposition, tissue remodeling, and anti-inflammatory activity, underscoring their importance as critical paracrine regulators in cartilage.[7,11,12]

Importantly, exosomes generally reflect the biological properties of their parental cells. Accumulating evidence indicates that exosomes derived from mesenchymal stem cells (MSCs) of different tissue origins exhibit distinct molecular cargo profiles and have specific therapeutic effects, depending on their source.[13,14] This tissue-specific heterogeneity has significant implications for the design of exosome-based therapies. While there is a growing body of literature supporting the use of MSC-Exos for cartilage repair, most existing studies have focused on exosomes derived from a single MSC source. Consequently, the therapeutic potential of combining exosomes from multiple MSC sources remains insufficiently explored.[6,15,16] In particular, there are few studies on the combined application of exosomes derived from human adipose-derived MSCs (hADSCs) and human umbilical cord-derived MSCs (hUCMSCs), despite the increasing interest in both cell sources.

Previous studies have suggested that hADSCs preferentially secrete bioactive factors associated with tissue regeneration, including signals involved in matrix synthesis, angiogenesis, and tissue remodeling, whereas hUCMSCs exhibit potent immunomodulatory properties that help regulate inflammation and immune responses.[17-19] These complementary biological features provide a rationale for exploring the therapeutic potential of exosomes derived from two sources. It is reasonable to hypothesize that exosomes isolated from hADSCs and hUCMSCs may retain source-specific functional attributes, and that their combination could offer a multifaceted therapeutic approach by simultaneously supporting regenerative processes and modulating the inflammatory microenvironment.

Therefore, the objective of the present study was to evaluate the therapeutic potential of a combined exosome formulation derived from hADSCs and hUCMSCs in a cartilage defect model, using untreated defects as controls. The present study was designed as a proof-of-concept investigation to assess the feasibility and regenerative efficacy of this combined cell-free approach, without focusing on in-depth mechanistic analyses.

Materials and Methods

Isolation of mesenchymal stem cell-derived exosomes

The UCMSCs and ADSCs were obtained from the Stem Cell Institute, University of Science, Vietnam National University at Ho Chi Minh city. The cells were originally isolated from human umbilical cord and adipose tissues and were collected under approved ethical protocols.

The MSCs used in this study were previously characterized for stemness by flow cytometry, showing positive expression (>95%) of CD44, CD73, CD90, and CD105, and negative expression (<2%) of CD14, CD34, CD45, and HLA-DR. In addition, their multipotency to differentiate into osteogenic, chondrogenic, and adipogenic lineages was confirmed under appropriate induction conditions. Cells (passage 4) were cultured at a density of 5,000 cells/cm^2 in tissue culture flasks using MSCCult I or ADSCCult I - FBS-free medium (Regenmedlab, Vietnam). The cultures were maintained at 37°C in a humidified atmosphere containing 5% CO_2.

The culture medium was replaced with fresh medium at 60%-70% confluency, and conditioned medium was collected after 48 h and stored at 4°C for up to one week before exosome isolation.

Exosomes were isolated using a differential ultracentrifugation protocol as previously described.[20] Briefly, the conditioned medium was centrifuged at 2,000 x g for 20 min at 4°C to remove cell debris and apoptotic bodies. The supernatant was centrifuged at 10,000 × g for 30 min at 4°C to remove large vesicles and debris, then filtered through a 0.22 µm filter. The filtrate was ultracentrifuged at 100,000 × g for 70 min at 4°C. The EV-containing pellet was resuspended in phosphate-buffered saline (PBS) and subjected to a second ultracentrifugation at 100,000 × g for 70 min using an Optima™ XE-90 ultracentrifuge (Beckman Coulter, USA). The extracellular vesicles (EVs) pellet, including exosome-enriched fractions, was resuspended in 100 µL of PBS and stored at 4°C. All EV preparations were used within 48h of isolation.

Quantification of exosomal protein content

Total protein concentration was quantified using the Bradford assay with Coomassie Brilliant Blue G-250 (Supelco, USA).[21] Human serum albumin standards (Albumin Standard, 23209, Thermo Fisher Scientific) were prepared at concentrations of 0.1, 0.25, 0.5, 0.75, 1.0, 1.2, and 1.4 mg/mL to generate a standard curve.

For each measurement, 5 µL of the relevant standard or EVs sample was mixed with 250 µL of Bradford reagent in a 96-well plate. Blank controls contained PBS instead of the protein sample. After incubation for 30 min at room temperature, the absorbance was measured at 595 nm using a microplate reader. All measurements were performed in triplicate, and protein concentrations were calculated based on the standard curve.

A combined EV formulation was prepared by mixing 50 µg of ADSC-derived EVs (ADSC-EVs)- and 50 µg of UCMSC-derived EVs (UCMSC-EVs) in 150 µL PBS, and stored at 4°C for up to 48 h before use.

Characterization of hMSC-derived exosomes by transmission electron microscopy (TEM)

The morphology of exosomes was examined by TEM. Freshly isolated EV samples were prepared and processed according to standard protocols. TEM analysis was performed at the National Institute of Hygiene and Epidemiology (NIHE, Vietnam) using a JEM-1400 Flash transmission electron microscope (JEOL, Japan) operated at 200 kV.

Nanoparticle Tracking Analysis (NTA)

Exosome size distribution and particle concentration were determined by NTA. Prior to the measurements, the sample chamber was flushed twice with PBS to remove residual particles, and a blank PBS sample was measured to record background particle levels. Exosome samples were diluted in PBS to a final volume of 400 µL and carefully loaded into the measurement chamber, avoiding air bubbles. The NTA measurements were performed using a ViewSizer 3000 system (HORIBA, Japan) according to the manufacturer's instructions and analyzed with ViewSizer software.[22]

Flow cytometric analysis of EV surface markers

The bead-based EV staining protocol used for flow cytometric analysis was performed according to the manufacturer's instructions, following a previously published method with modifications.[23]

The surface markers of exosomes were analyzed by flow cytometry using a bead-based assay. Briefly, EVs (10 µg) were incubated with 1 µg of latex beads (Gibco, Thermo Fisher Scientific) in PBS (final volume, 1 mL) for 2h at room temperature or overnight at 4°C. The reaction was quenched by adding 100 µL of 1M glycine (Sigma-Aldrich, USA) and incubating for 30 min at room temperature. Bead-EV complexes were collected by centrifugation at 10,000 rpm for 5 min, washed twice with PBS containing 0.5% bovine serum albumin (BSA), and incubated with antibodies against CD9, CD63, and CD81 (Gibco, USA) for 30 min at 4°C. The labeled samples were analyzed using a FACS Melody flow cytometer (BD Biosciences, USA).

The effect of exosomes on chondrogenic differentiation of MSCs

ADSCs were seeded at a density of 5x10^3 cells/cm^2 in six-well plates and cultured to 80-90% confluence. Chondrogenic differentiation was induced using StemPro™ Chondrogenesis Differentiation Medium (Gibco, USA) and maintained for 21 days, with the medium changed weekly. For *in vitro* treatments, a combined EV formulation consisting of 50 µg of hADSC-EVs (10^{10} particles) and 50 µg of hUCMSC-EVs (10^{10} particles) suspended in 150 µL of PBS was administered once at the initiation of chondrogenic induction. The control group received 150 µL of PBS alone.

Animal model of cartilage defects

Female Wistar rats (8-9 weeks old, 150-200 g) were housed under standard laboratory conditions and given free access to food and water.

A full-thickness cartilage defect was surgically created in the medial femoral condyle (1.4 mm in diameter × 1.0 mm in depth). The rats were anesthetized with xylazine (7 mg/kg) and zoletil (7 mg/kg). A total of 100 µg of EVs (10^{10} particles per EV source) in 150 µL of PBS or PBS alone was administered directly into the defect site. The animals were humanely euthanized with an overdose of anesthesia at 1, 4, 8, and 12 weeks post-surgery. Cervical dislocation was subsequently performed by trained personnel as a secondary physical method to ensure death. Adequate depth of anesthesia was confirmed prior to the procedure. Death was verified by the absence of cardiac and respiratory activity. All procedures were conducted in accordance with the AVMA Guidelines for the Euthanasia of Animals.

Acute and subacute toxicity was evaluated based on mortality, clinical signs, and behavioral changes during the first seven days following EV administration.

Radiographic and macroscopic evaluation

Radiographic evaluation was performed using the In Vivo Xtreme II imaging system (Bruker, USA). The images were acquired at predetermined time points using an X-ray setting of 35 kVp with an exposure time of 15 s.

Macroscopic assessment of cartilage repair was conducted immediately after sample harvest using Goebel's semi-quantitative macroscopic scoring system.[24] The evaluation comprised five parameters: (1) color of the repair tissue, (2) presence of vascularization, (3) surface integrity, (4) degree of defect filling, and (5) degeneration of the adjacent articular cartilage.

Histological and immunofluorescence analyses

Femoral condyle samples were harvested at predetermined time points and fixed in 4% paraformaldehyde for 24 h. The specimens were decalcified in 10% EDTA solution for two weeks with regular solution changes, dehydrated, embedded in paraffin, and sectioned at 4 µm. For histological evaluation, the paraffin-embedded sections were deparaffinized, rehydrated, and stained with hematoxylin and eosin (H&E) to assess general morphology, with Safranin-O/Fast Green to measure the proteoglycan content, and Masson's trichrome (ab150686, Abcam) to visualize collagen deposition, following standard staining protocols. After staining, the sections were dehydrated using a graded ethanol series, cleared in xylene, and mounted for microscopic examination. Semi-quantitative analysis of the percentage of Safranin O- and collagen-positive areas was performed using at least three independent biological replicates (n = 3), each analyzed in duplicate (technical replicates).

For immunofluorescence analysis, the deparaffinized and rehydrated sections were subjected to indirect immunofluorescence staining. Briefly, the sections were incubated with a primary antibody against aggrecan (MA3-16888) followed by Alexa Fluor 488-conjugated secondary antibody (Invitrogen). Nuclei were counterstained where applicable, and slides were mounted with antifade medium. Fluorescent images were captured using a fluorescence microscope under identical acquisition settings.

Indirect immunofluorescence staining

The paraffin-embedded sections were deparaffinized and rehydrated through a graded ethanol series. The sections were incubated with a primary antibody against aggrecan (MA3-16888) for 30 min at room temperature in the dark. After washing twice with PBS for 5 min each to remove unbound antibodies, the sections were incubated with a goat anti-mouse Alexa Fluor 488-conjugated secondary antibody (Invitrogen; 1:200) for 30 min at room temperature in the dark. The sections were then washed twice with PBS, mounted with coverslips, and stored away from the light until imaging.

RNA extraction and quantitative RT-PCR

Articular cartilage tissues were harvested from the surgically treated knees of rats in the exosome-treated group, while cartilage from the contralateral non-operated knees served as normal controls (n = 3 per group). Approximately 130 mg of cartilage tissue was collected, immediately transferred into 1.5 mL tubes containing 1 mL of easy-BLUE™ Total RNA Extraction reagent (iNtRON Biotechnology, Korea), and processed according to the manufacturer's instructions.

Total RNA was isolated and used for quantitative reverse transcription–polymerase chain reaction (RT-qPCR) analysis using the Luna® Universal One-Step RT-qPCR Kit (New England Biolabs, USA). The gene-specific primers used for RT-qPCR are listed in Table 1.

Relative gene expression levels were normalized to glyceraldehyde-3-phosphate dehydrogenase (GAPDH)

Table 1. Primer sequences used for RT-qPCR

Seq. Name	Forward	Reverse	Ref
rTNF-α	GGCCAATGGCATGGATCTCAAA	AGCCTTGTCCCTTGAAGAGAACCT	10.1074/jbc.M112.368639
rIL1-β	ACCTGCTAGTGTGTGATGTTCCC	GCTTTCAGCTCACATGGGTCAGA	10.1074/jbc.M112.368639
rIFN-γ	CATCGCCAAGTTCGAGGTGAAC	TGGTGACAGCTGGTGAATCACTCT	10.1074/jbc.M112.368639
rACAN	CTTGGGCAGAAGAAAGATCG	GTGCTTGTAGGTGTTGGGGT	10.3390/cells12182222
rCOL2	AAGTCACTGAACAACCAGATTGAGA	AAGTGCGAGCAGGGTTCTTG	10.1038/s41598-017-16902-4
rSOX9	CCCGATCTGAAGAAGGAGAGC	GTTCTTCACCGACTTCCTCCG	10.1177/1947603519870862
rPRG4	CTACAACAGCTTCTGCGAAGAA	GATTTGGGTGAACGTTTGGTGG	10.3390/ijms17030359
rCOMP	GCAGACAAGGTGGTAGACAAGA	GCCTGGGTCGCTGTTCATT	10.7150/jca.49144
rMMP13	GATGACCTGTCTGAGGAAGACC	GCATTTCTCGGAGCCTGTCAAC	10.2147/DDDT.S397185
rADAMTS5	AGAGTCCGAACGAGTTTACG	GTGCCAGTTCTGTGCGTC	10.3892/mmr.2022.12688
rRUNX2	AACTTGCTAACGTGAATGGTC	TAGCCCACTGAAGAAACTTGG	10.1016/j.bioactmat.2021.04.013
rWNT5A	ATTCTTGGTGGTCGCTAGGTA	CGCCTTCTCCGATGTACTGC	10.18632/oncotarget.10846
rCOL10	AGGCACTAAAGGTGAGACACGT	CAACAAGACCTCGAAGACCAG	10.1016/j.joca.2014.07.028
rGAPDH	CAATTCCATCCCAGACCCCAT	GGTGCAGCGAACTTTATTGAT	Primer-Blast (NCBI) XM_063285519.1

as a reference gene using the ΔCt method and calculated relative to the control group using the $2^{-\Delta\Delta Ct}$ method.[25]

Statistical analysis

All quantitative data are presented as mean ± standard deviation (SD). Statistical analyses were performed using GraphPad Prism software (version 8.0.2; GraphPad Software, USA). Comparisons between two groups were conducted using an unpaired two-tailed Student's t-test. For comparisons involving multiple time points, the data were analyzed using one-way analysis of variance (ANOVA) followed by appropriate post hoc tests where applicable. Macroscopic scoring data were analyzed using non-parametric statistical methods due to their ordinal nature. A value of $P < 0.05$ was considered statistically significant.

Results

Characterization of hMSC-derived exosomes

Transmission electron microscopy revealed that the exosomes isolated from ADSC and UCMSC culture supernatants exhibited a typical cup-shaped morphology and were predominantly distributed within the 30-200 nm size range (Fig. 1). Nanoparticle tracking analysis demonstrated that the ADSC-EVs had a mean diameter of 117.08 ± 7.10 nm, with 90% of particles below 188.59 ± 7.17 nm (Fig. 1A), whereas UCMSC-EVs showed a mean diameter of 91.12 ± 5.54 nm and a D90 value of

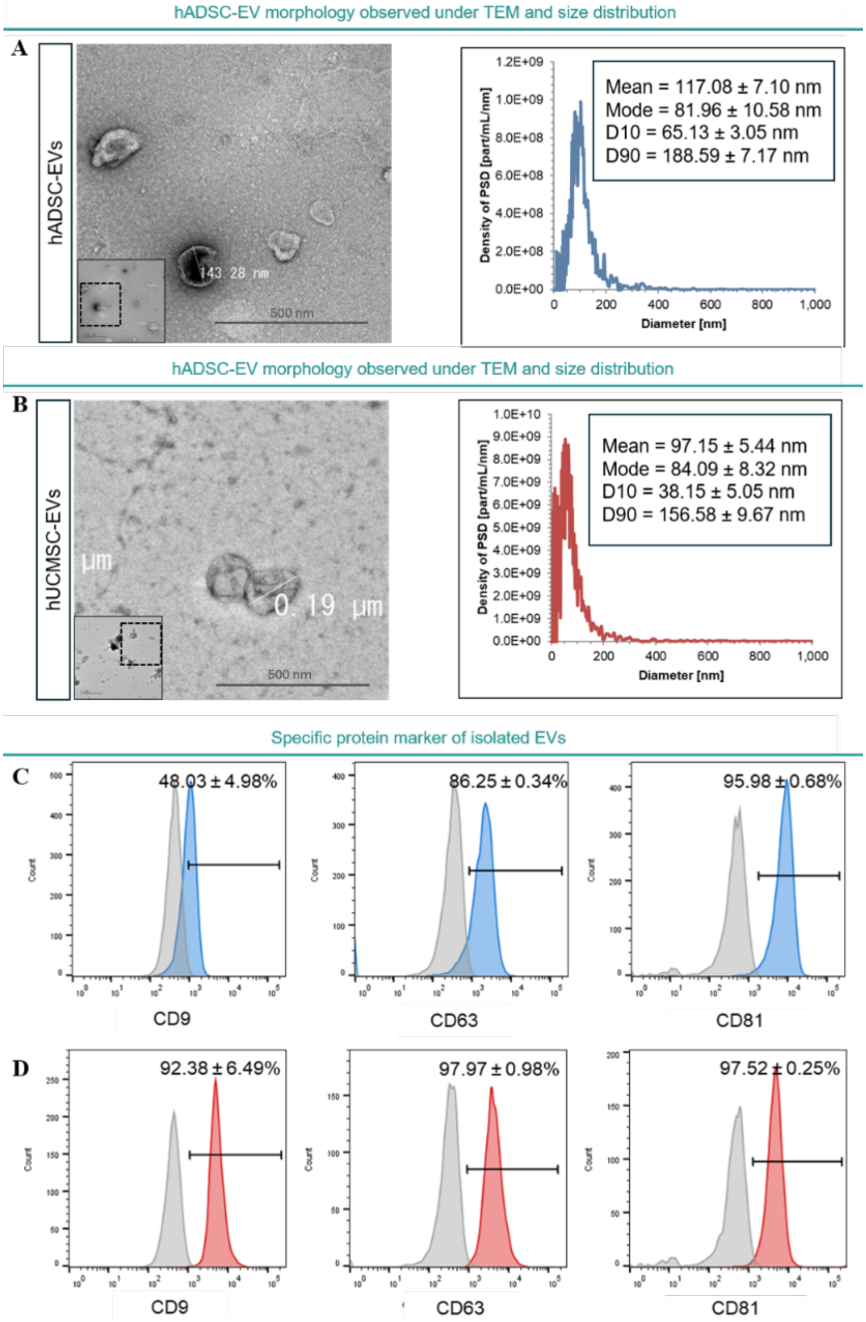

Fig 1. Characterization of exosomes derived from mesenchymal stem cells. (A, B) Transmission electron microscopy (TEM) images showing the typical cup-shaped morphology and size distribution of exosomes isolated from ADSC-EVs and UCMSC-EVs. Scale bar = 500 nm; (C, D) Flow cytometric analysis of tetraspanin surface markers CD9, CD63, and CD81 on exosomes isolated from ADSC and UCMSC conditioned media. Fluorescence intensity of CD9-FITC, CD63-PE, and CD81-APC is shown on the x-axis, and event count is shown on the y-axis (n = 3 biological replication).

156.58 ± 9.67 nm (Fig. 1B). Despite the asymmetric size distributions, the groups exhibited comparable modal diameters.

Flow cytometric analysis confirmed the expression of canonical exosomal markers. The ADSC-EVs expressed CD9, CD63, and CD81 at 64.39% ± 0.85%, 86.87% ± 0.08%, and 95.99% ± 0.56%, respectively (Fig. 1C), while UCMSC-EVs showed higher expression levels of CD9 (93.47% ± 5.46%), CD63 (98.16% ± 1.08%), and CD81 (97.64% ± 0.31%) (Fig. 1D). These results confirmed that the isolated nanoparticles met the morphological, size, and surface marker criteria of exosomes. In this study, the terms "UCMSC-EVs" and "ADSC-EVs" are used to refer to exosome-enriched EV fractions derived from UCMSCs and ADSCs, respectively.

Effects of exosome-enriched EV fractions on chondrogenic differentiation of ADSCs in vitro

The mesenchymal stem cells used in this study exhibited multilineage differentiation potential, as previously reported (Fig. 2A). Following culture in chondrogenic induction medium with or without EV supplementation,

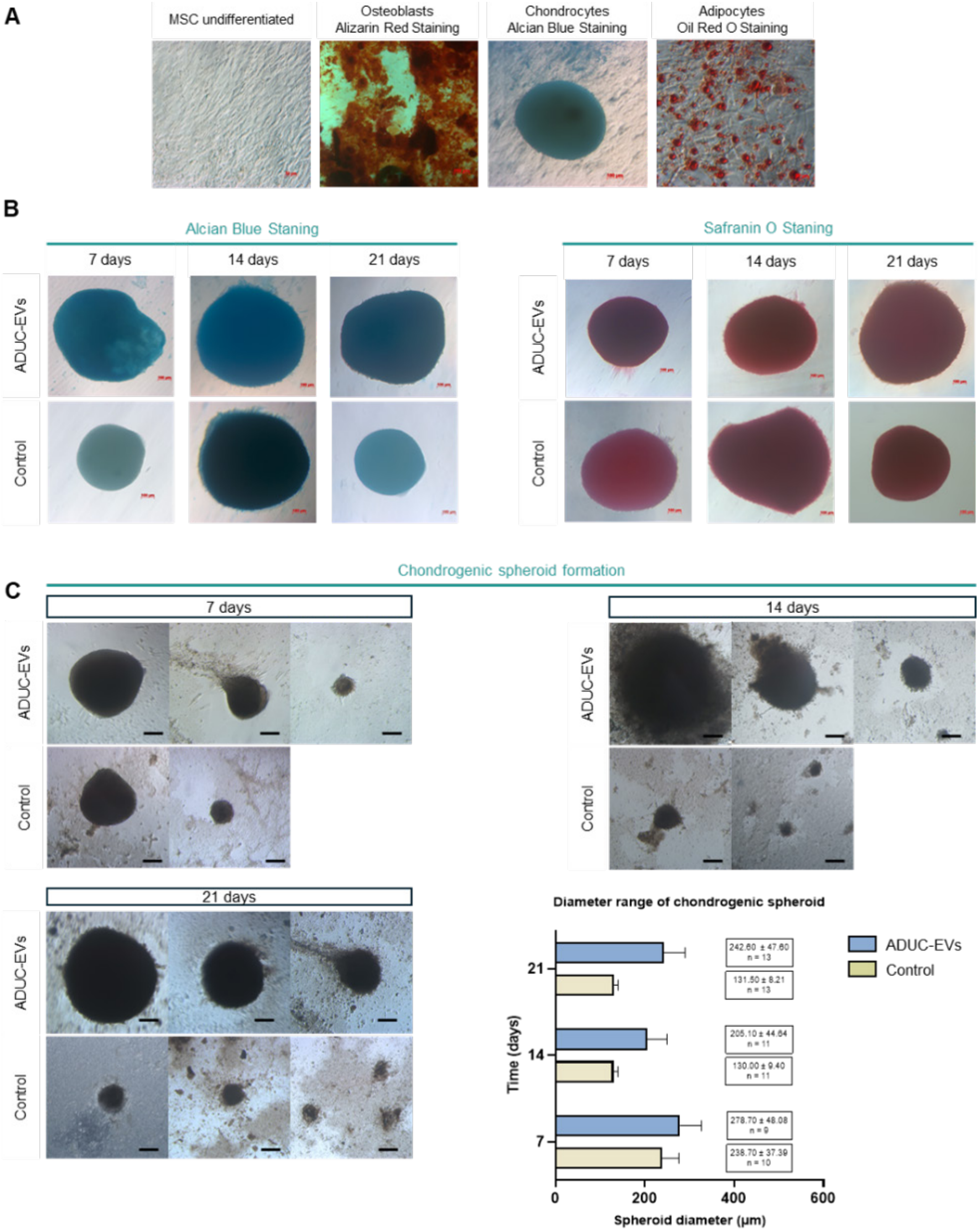

Fig. 2. EVs-enhanced chondrogenic differentiation of ADSCs. (A) Multipotent differentiation capacity of ADSCs into osteogenic, chondrogenic, and adipogenic lineages, as demonstrated by Alizarin Red S, Alcian Blue, and Oil Red O staining, respectively (n = 3 biological replication). (B) Enhanced chondrogenic differentiation of ADSCs in the presence of combined EVs, as indicated by increased proteoglycan deposition detected by Alcian Blue staining (left) and Safranin O staining (right) at days 7, 14, and 21 of induction (n = 3 biological replication). (C) Representative images of chondrogenic spheroid formation (scale bar = 100 μm) and quantitative analysis of mean spheroid diameter of differentiating ADSCs at the indicated time points(n = 3 biological replication, The number of spheroids is shown, and spheroid diameter was measured in two technical replicates).

chondrogenic differentiation was evaluated at days 7, 14, and 21 using Alcian Blue and Safranin O staining. Undifferentiated ADSCs showed minimal staining, whereas chondrogenic induction resulted in progressive proteoglycan deposition over time (Fig. 2B).

The EV-treated cultures consistently exhibited enhanced chondrogenic spheroid formation and stronger Alcian Blue and Safranin O staining compared to the controls (Fig. 2B). After 21 days, the spheroids in the EVs-treated group displayed a significantly larger mean diameter (242.6 ± 171.6 μm) with a broader size distribution, whereas the control spheroids were smaller and more uniform in size (131.5 ± 29.6 μm) (Fig. 2C). These findings indicate that EV supplementation enhanced chondrogenic differentiation of ADSCs *in vitro*.

Development of a rat model of cartilage defects

The contralateral non-operated knee of each rat served as the internal normal control (Fig. 3). Macroscopic examination of native femoral condyle cartilage revealed a smooth, glistening surface without visible defects or osteophyte formation. Standardized osteochondral defects were successfully created in the medial femoral condyle (Fig. 3A).

All animals recovered rapidly following surgery and resumed normal ambulation within 24 hours, including those that did not receive the EVs treatment. No signs of acute hypersensitivity reactions were observed within three days post-surgery, and no mortality occurred during the seven-day postoperative observation period. In addition, no postoperative infections or wound complications were detected (Fig. 3B).

The target defect diameter was 1.4 mm, and the measured defect diameter was 1.49 ± 0.08 mm (n = 18), corresponding to a defect area of 1.74 ± 0.18 mm^2 (data not shown) (Fig. 3C). This minor deviation was attributed to procedural and instrumental variability and was considered acceptable and reproducible under the experimental conditions.

Body weight was monitored daily for seven days after surgery to assess postoperative recovery (Fig. 3D). There were no significant differences in body weight trends between the PBS- and EV-treated groups, and no postoperative weight loss was recorded in either group. Final body weight gain did not differ significantly between the control group (17.78 ± 3.73 g) and the EVs group (16.00 ± 13.39 g) (n = 9, $P > 0.05$).

Macroscopic and radiographic evaluation of cartilage repair

Macroscopic assessment

At one week post-surgery, repair tissue minimally

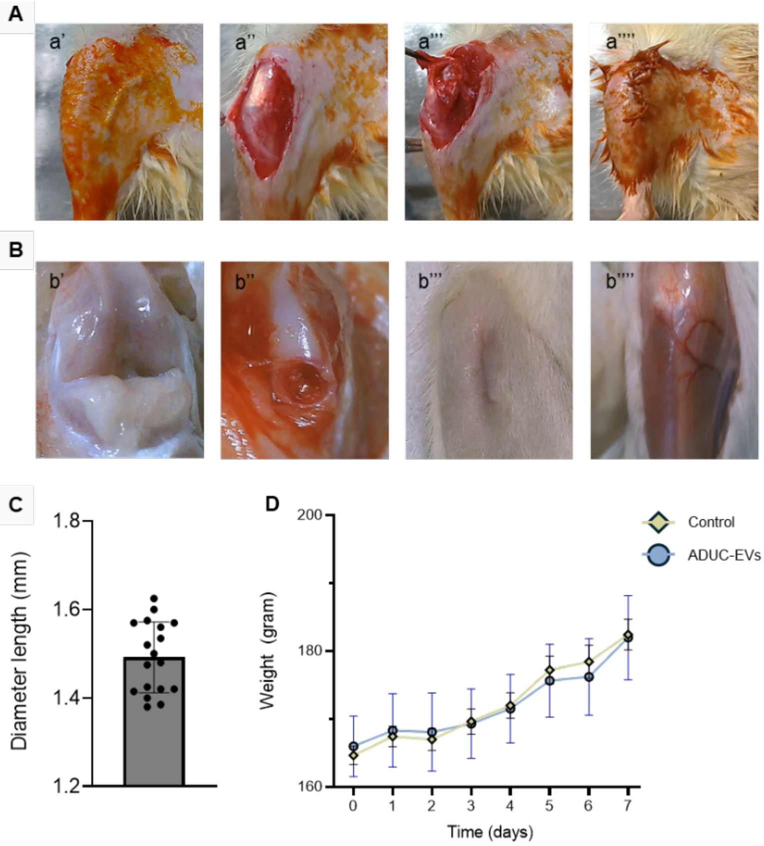

Fig. 3. Establishment of a rat femoral condyle cartilage defect model and postoperative evaluation. (A) Schematic illustration of the surgical procedure used to create an articular cartilage defect in the medial femoral condyle of rats. (B) Representative macroscopic images showing native articular cartilage with a smooth, glistening surface and the absence of defects or osteophytes (b'). In defect-induced joints, cartilage erosion and/or osteophyte formation were observed at the medial femoral condyle following surgery (b''). Complete wound closure and normal healing of the surgical site were evident within one week post-surgery (b''', b''''). (C) Quantitative assessment of the initial defect size in the medial femoral condyle, with an average diameter of 1.49 ± 0.08 mm (n = 18 biological replication). (D) Postoperative body weight changes in PBS- and EVs-treated groups over time. Data are presented as mean ± standard error of the mean (SEM) (n = 9 rats per group).

covered the cartilage defects in both groups, accompanied by sparse neovascularization (Fig. 4A). The color of the defect area was clearly distinguishable from that of the adjacent native cartilage. At four and eight weeks, approximately 50% defect coverage was observed in both groups; however, the EV-treated group exhibited a smoother surface and more pronounced vascularization compared to the control group. By 12 weeks post-surgery, continuous defect coverage was observed in both groups, with the EVs group showing a smoother, more homogeneous surface, whereas the control group displayed an irregular and heterogeneous appearance.

Semi-quantitative macroscopic evaluation using Goebel's scoring system revealed no significant difference between groups at one week post-surgery ($n=3$, $P=0.68$). However, the EVs-treated group demonstrated progressively improved scores compared to the control group at later time points, including four weeks (11.7 ± 0.58 vs 9.0 ± 1.0) ($n=3$, $P=0.0007$), eight weeks (10.0 ± 0.0 vs 7.3 ± 0.58) ($n=3$, $P=0.007$), and 12 weeks (9.3 ± 0.58 vs 2.3 ± 0.58) ($n=3$, $P<0.001$) (Fig. 4B). As lower scores indicate closer resemblance to native cartilage, these results suggest enhanced macroscopic cartilage repair in the EVs-treated group over time.

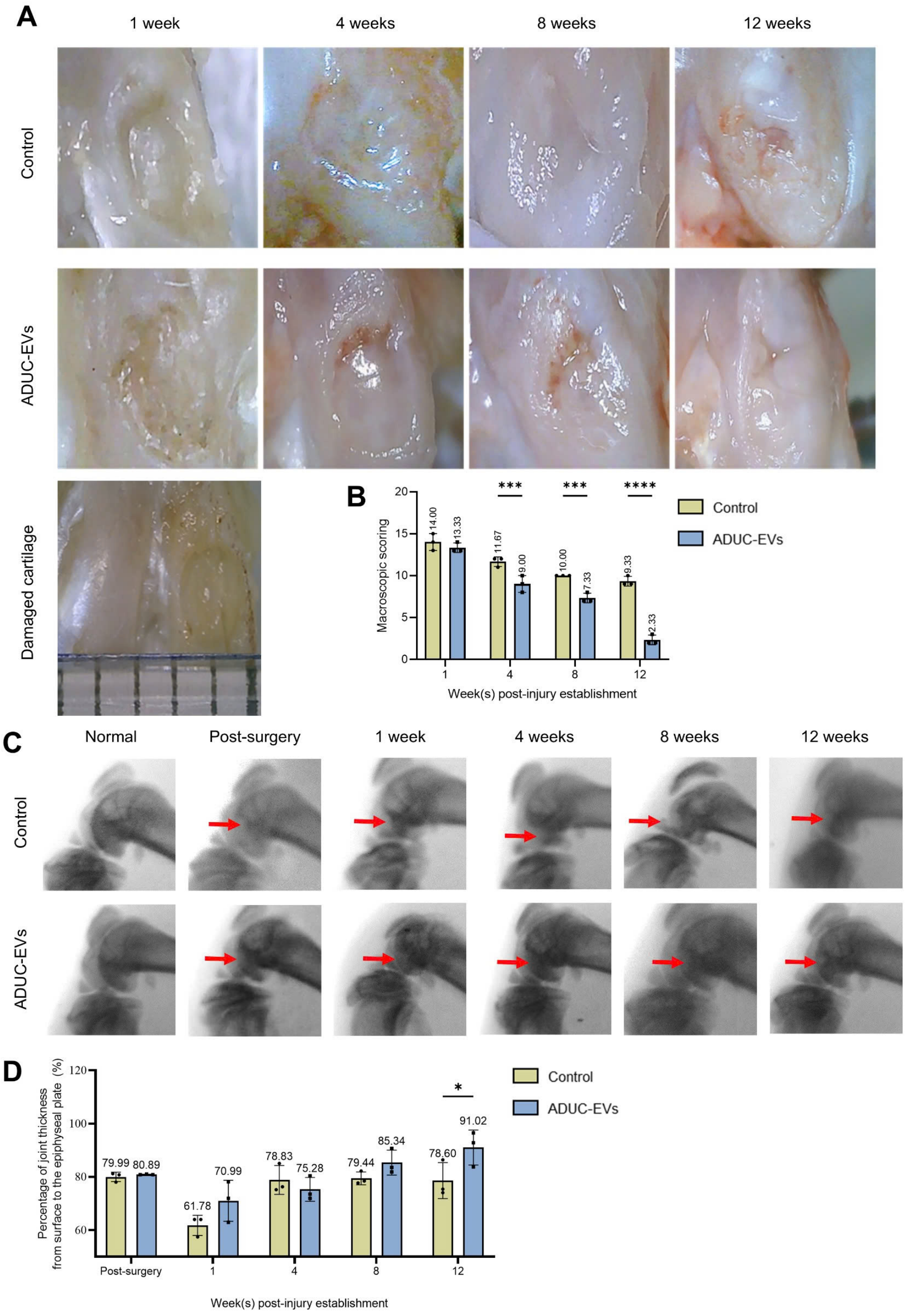

Fig. 4. Macroscopic evaluation of cartilage regeneration. (A) Representative macroscopic images of cartilage defects at 1, 4, 8, and 12 weeks post-surgery, showing progressive surface coverage and defect filling in both groups; (B) Quantitative assessment of cartilage regeneration using the macroscopic scoring system described by Goebel et al.; (C) X-ray images demonstrating gradual filling of cartilage defects (red arrows) over time in both groups. (D) Quantification of joint thickness revealed limited regenerative capacity up to 12 weeks post-surgery. Data are presented as mean ± SD ($n=3$). *$P<0.05$, **$P<0.01$, ***$P<0.001$.

Radiographic evaluation

Radiographic analysis revealed intact articular cartilage with a smooth surface and a clearly defined epiphyseal plate in non-operated joints. At one week post-surgery, both groups exhibited defect enlargement relative to the initial defect size (Fig. 5A). Repair tissue with higher radiodensity than the surrounding cartilage progressively filled the defect region over time in both groups. However, neither group achieved complete defect filling at 12 weeks post-surgery.

The thickness of the articular cartilage was quantified by measuring the distance between the repair tissue surface and the epiphyseal plate and expressed as a percentage relative to the contralateral normal cartilage (defined as 100%). At baseline, the cartilage thickness ratios were comparable between the control and EV groups (79.99 ± 1.75% vs 80.89 ± 0.12%) (n = 3, $P = 0.9998$). At one week post-surgery, the ratios had decreased to 61.78 ± 3.79% and 70.99 ± 7.68% in the PBS and EV groups (n = 3, $P = 0.1546$), respectively, reflecting early

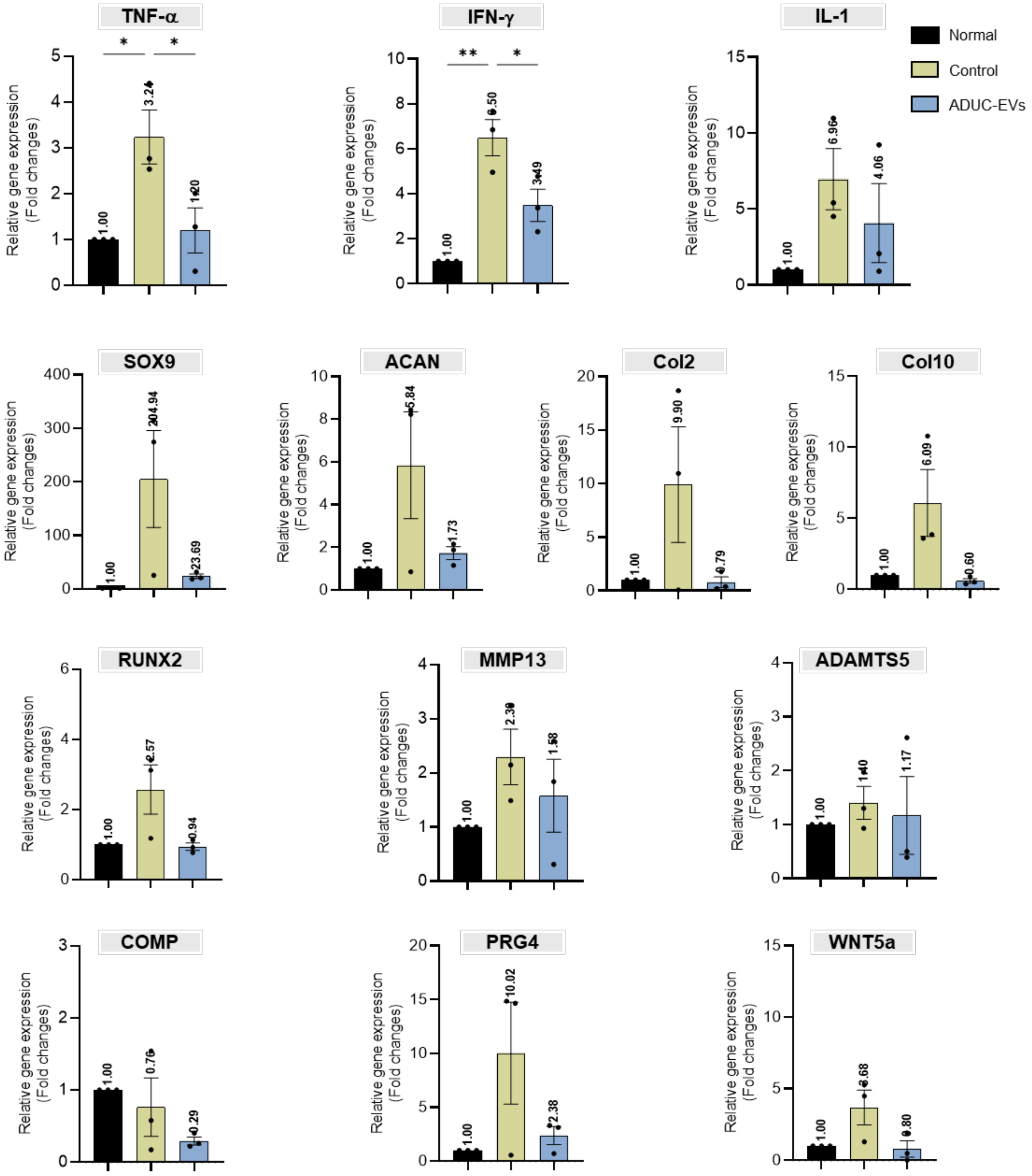

Fig. 5. RT-qPCR analysis of chondrogenic-related gene expression in experimental cartilage. Relative mRNA expression levels of inflammatory cytokines (TNF-α, IFN-γ, IL-1β), chondrogenic markers (SOX9, ACAN, COL2), hypertrophic markers (RUNX2, COL10), extracellular matrix-related genes (COMP, PRG4), and catabolic enzymes (MMP13, ADAMTS5, WNT5A) were quantified by RT-qPCR. Gene expression levels were normalized to GAPDH and expressed as fold change relative to normal cartilage tissue. The yellow bars represent the PBS-treated group, and the blue bars represent the EV-treated group. Data are presented as mean ± SEM (n = 3 biological replication, One-way ANOVA). * $P < 0.05$, ** $P < 0.01$.

defect expansion. At 4, 8, and 12 weeks post-surgery, the cartilage thickness in the control group remained similar to the baseline levels (78.60 ± 6.76%), whereas the EV-treated group showed a progressive increase, reaching 91.02 ± 6.57% at 12 weeks (n = 3, *P* = 0.0288).

Quantitative reverse transcription–polymerase chain reaction analysis of the chondrogenic potential of EV-enriched exosome fractions in a rat model

Quantitative RT-PCR analysis revealed a pronounced inflammatory response at one week post-injury in both groups, as indicated by the increased expression of the proinflammatory cytokines *TNF-α*, *IFN-*, and *IL-1β* (Fig. 5). However, this upregulation was markedly attenuated in the EV-treated group. Specifically, the *TNF-α*, *IFN-γ*, and *IL-1β* expression levels in the control group increased by 3.24-, 6.50-, and 6.96-fold, respectively, whereas the corresponding increases in the EV-treated group were limited to 1.20-, 3.49-, and 4.06-fold, indicating a suppressive effect of EV-enriched exosomes on early inflammatory signaling.

Analysis of cartilage-associated genes showed differential expression patterns between groups. *WNT5A* and *COL2A1* were markedly upregulated in the control group (3.68- and 9.90-fold, respectively), while their expression remained unchanged or was downregulated in the EV-treated group (0.80- and 0.79-fold, respectively). *ACAN* expression increased in both groups, but was more pronounced in the control group (5.84-fold) compared to the EVs group (1.73-fold).

The expression levels of key transcription factors and matrix markers were examined to assess chondrogenic commitment versus hypertrophic differentiation. In the control group, *SOX9* and *COL2A1* were strongly upregulated (204.94- and 9.90-fold, respectively), accompanied by increased expression of the hypertrophic markers *RUNX2* (2.57-fold) and *COL10A1* (6.09-fold). In contrast, EV treatment resulted in moderate upregulation of *SOX9* (23.69-fold), while *COL2A1*, *RUNX2*, and *COL10A1* were downregulated (0.79-, 0.94-, and 0.60-fold, respectively), suggesting attenuation of chondrocyte hypertrophy at the early repair stage.

Extracellular matrix-related genes showed a general downregulation at seven days post-surgery. *COMP* expression was decreased in both the control (0.76-fold) and EV-treated groups (0.29-fold). Similarly, *PRG4* expression was reduced in the EV group compared to the control group. Finally, the catabolic enzymes *MMP13* and *ADAMTS5* were upregulated in the control group (2.30- and 1.40-fold, respectively), whereas their expression levels in the EV-treated group were lower (1.58- and 1.47-fold), indicating reduced matrix-degrading activity following EV administration.

Histological evaluation of cartilage repair

Normal rat articular cartilage exhibited the typical zonal organization and abundant extracellular matrix (ECM), as confirmed by H&E, Masson's trichrome, and Safranin-O/Fast green staining (Fig. 6A). Collagen-rich regions were visualized by Masson's trichrome, while the distribution of glycosaminoglycans (GAGs) was identified by Safranin-O staining.

At one week post-surgery, H&E staining revealed that the defect areas in both groups were predominantly filled with fibroblast-like cells characterized by an elongated, spindle-shaped morphology, accompanied by the presence of small blood vessels (Fig. 6B). Masson's trichrome staining demonstrated the deposition of mixed collagenous and non-collagenous matrix at the repair site, while Safranin-O staining indicated a scattered presence of GAGs in both groups, suggesting an early reparative response involving heterogeneous cell populations.

By four weeks post-surgery, chondrocyte-like cells were evident in the repair tissue, with a concomitant reduction in fibroblast-like cells in both groups. Vascular structures were still detectable but were less prominent. In the control group, collagen deposition was localized around cell-rich regions, whereas GAG staining was weak and largely confined to the defect surface. In contrast, the EV-treated group showed comparable collagen deposition, but there was minimal GAG staining on the defect surface (Fig. 6B).

At eight weeks post-surgery, continued defect repair was observed in both groups, with the emergence of hyaline cartilage-like tissue. The control group displayed surface hyperproliferation, whereas the EV-treated group exhibited a smoother surface morphology. Collagen deposition was present in both groups but remained irregularly distributed. Notably, GAG-positive but collagen-negative staining was detected on the defect surface in the EV-treated group, while the control group showed collagen-positive but GAG-negative surface staining (Fig. 6B).

At 12 weeks post-surgery, histological features were largely consistent with those observed at eight weeks. The control group continued to show surface hyperproliferation and persistent vascularization, whereas vascular structures were rarely detected in the EV-treated group. Collagen staining in the control group remained uneven and was largely localized to cell-dense areas, while in the EV-treated group, collagen deposition was predominantly distributed along the defect surface. Similarly, GAG staining in the control group was limited to pericellular regions, whereas the EV-treated group exhibited a broader extracellular GAG distribution that colocalized with collagen-rich areas (Fig. 6B).

Semi-quantitative image analysis revealed no significant differences in collagen- or GAG-positive areas between groups at one and four weeks post-surgery. At eight weeks, collagen and GAG coverage remained comparable between the control and EV-treated groups. In contrast, at 12 weeks post-surgery, the EV-treated group demonstrated significantly higher collagen-positive (78.76 ± 10.55%) and GAG-positive areas (58.24 ± 14.01%) compared to the control group (57.53 ± 3.92%) (n = 3, *P* = 0.0308) and 27.29 ± 3.40% (n = 3, *P* = 0.0205), respectively; (Fig. 6C).

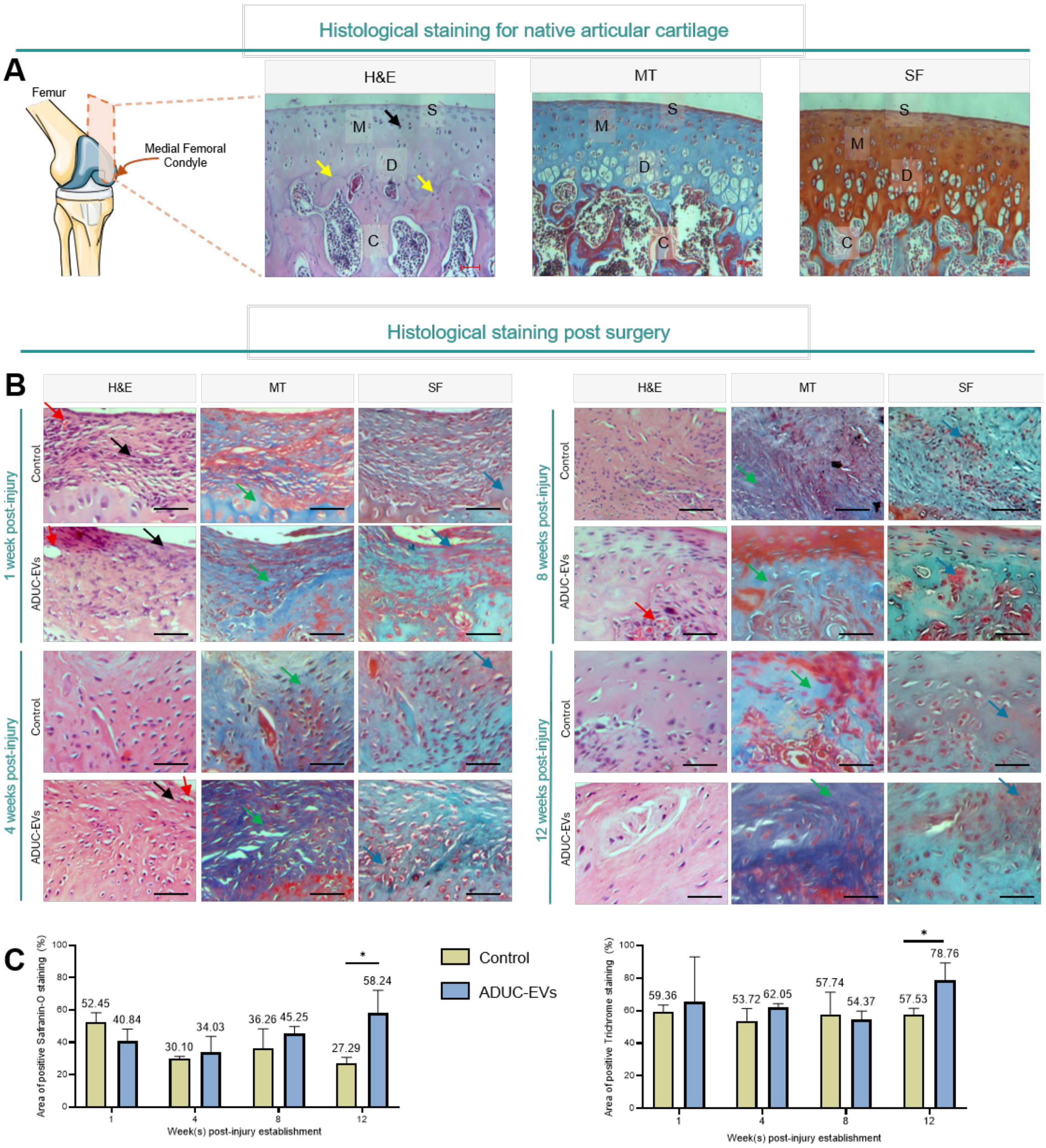

Fig 6. Histological evaluation of articular cartilage repair in the rat medial femoral condyle. (A) Representative histological images of normal rat articular cartilage stained with hematoxylin and eosin (H&E), Masson's trichrome, and Safranin-O/Fast Green, showing the characteristic zonal organization of mature cartilage, including the superficial (S), middle (M), and deep (D) zones. The calcified cartilage (C) is separated from the deep zone by the tidemark (yellow arrow) and lies directly above the subchondral bone (magnification × 20; scale bar = 50 µm). (B) Representative histological sections of cartilage defects at 1, 4, 8, and 12 weeks post-injury in the control and EV-treated groups (scale bar = 50 µm). The black arrows indicate fibroblast-like cells; the red arrows indicate small blood vessels; the green arrows indicate collagen-positive areas, and the blue arrows indicate glycosaminoglycan (GAG)-positive areas. (C) Quantitative analysis of GAG-positive (left) and collagen-positive (right) areas at 1, 4, 8, and 12 weeks post-surgery. Data are presented as mean ± SD (n = 3 biological replication, $*P < 0.05$).

Overall, collagen deposition in the control group showed a declining trend, whereas EV treatment was associated with improved matrix accumulation at later stages of repair.

Immunofluorescence analysis of aggrecan distribution during cartilage repair

Aggrecan distribution at the defect sites was examined by indirect immunofluorescence staining at one and 12 weeks post-surgery, with cell nuclei counterstained using Hoechst 33342 (Fig. 7). In normal articular cartilage, aggrecan was predominantly distributed in the superficial and middle zones, with lower expression in the deep and calcified zones.

At one week post-surgery, the control group exhibited a high density of proliferating cells on the defect surface. Aggrecan immunoreactivity was primarily localized around these proliferating cells and was sparsely detected in regions containing hypertrophic cells. In contrast, the EV-treated group showed fewer proliferating cells at the defect surface, while aggrecan expression was more prominently and uniformly distributed across the defect area.

At 12 weeks post-surgery, the number of cells within the

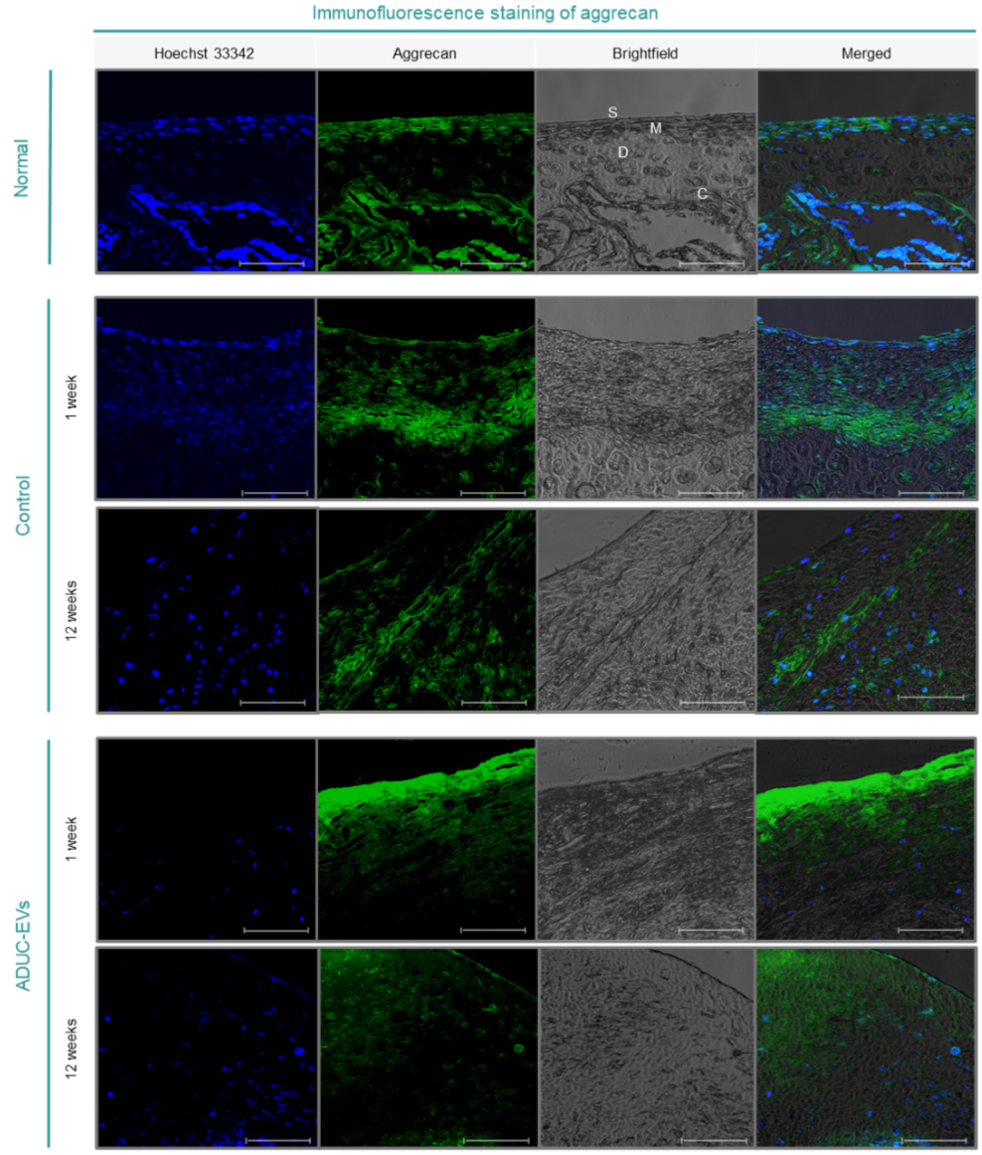

Fig 7. Indirect immunofluorescence staining of articular cartilage post-surgery in a rat model. Characterization of aggrecan post-surgery. Normal articular cartilage was used as a visual standard for immunofluorescence staining. Articular cartilage is organized into four zones: superficial zone (S), middle zone (M), deep zone (D), and calcified zone (C). Magnification X40, scale bar = 75 μm

repair tissue decreased in the control group but increased in the EV-treated group compared with the one-week time point. In the control group, aggrecan expression appeared heterogeneous and was confined to discrete regions within the repair tissue. Conversely, in the EV-treated group, aggrecan was more evenly distributed throughout the defect area, regardless of local cell density, indicating a more homogeneous extracellular matrix organization at the later stage of repair.

Discussion

Articular cartilage has limited intrinsic regenerative capacity, and untreated focal defects frequently progress toward degenerative joint disease. Effective cartilage repair, therefore, requires the coordinated regulation of inflammation responses, extracellular matrix (ECM) remodeling, and chondrocyte differentiation, rather than simple defect filling or excessive cellular proliferation.[6,26]

Exosomes have emerged as key mediators of intercellular communication and tissue regeneration due to their ability to deliver bioactive cargos that modulate cellular behavior in a context-dependent manner.[27,28] ADSC- EVs have been reported to enhance chondrocyte proliferation, extracellular matrix synthesis, and cell survival through microRNA-mediated signaling pathways, including miR-429-associated mechanisms.[27-29] In parallel, UCMSC-EVs have demonstrated regulatory effects on chondrocyte migration, apoptosis, and inflammatory signaling, particularly IL-1-driven response, as well as macrophage polarization.[30-32] These complementary biological properties provided the mechanistic rationale for the present study’s evaluation of a combined ADSC-EVs and UCMSC-EVs strategy for cartilage defect repair.

Exosome-enriched EVs were isolated by ultracentrifugation and characterized by morphology, size distribution, and the expression of canonical tetraspanin markers (CD9, CD63, and CD81). High expression of CD63 and CD81 was consistently detected in both ADSC-EVs and UCMSC-EVs preparations, consistent with previous reports describing their involvement in exosome biogenesis, cargo sorting, and cellular uptake.[33-36] Although these markers primarily serve to validate exosome identity, their presence is also consistent with the isolated vesicles' capacity to participate in active intercellular signaling within an inflammatory microenvironment.[37] Another important aspect of EV-based therapeutic strategies is the variation in EV dosing across studies. In rat models of cartilage defects, reported doses vary widely, ranging from 10^7 to 10^{10} particles per treatment.[38-41] In this study, the concentration of EVs isolated from MSCs was within the reported range and was considered appropriate relative to the total volume of conditioned culture supernatant used for EV isolation.

Cartilage regeneration is highly sensitive to the inflammatory milieu during the early post-injury phase. Proinflammatory cytokines such as *TNF-α* and *IL-1β* are known to activate catabolic signaling cascades, including WNT5A-dependent pathways, leading to upregulation of matrix-degrading enzymes such as *MMP13* and *ADAMTS5*.[42,43] Consistent with previous studies, both *in vitro* and *in vivo* OA models treated with ADSC-derived EVs at different concentrations (reported by Chang Hee Woo et al. (1×10^8 particles/mL) and Miguel Tofiño-Vian et al (7.2×10^7 particles/mL)) demonstrated reduced *IL-1β* expression. These findings suggest that exosome-enriched EVs derived from ADSCs can attenuate inflammatory signaling and modulate cartilage degradation.[39,40] In contrast, Zhou et al reported a significant reduction in the pro-inflammatory cytokine *IL-1β* in OA models following treatment with UCMSC-derived exosome-enriched EVs (10 µL at $1\text{x}10^{11}$ particles/mL), resulting in the inhibition of *ADAMTS5* and *MMP13* expression.[38] In line with these findings, untreated defects exhibited early and widespread upregulation of inflammatory and catabolic gene expression. In contrast, EV-treated defects exhibited reduced expression of pro-inflammatory cytokines along with downregulation of key catabolic genes (*MMP13* and *ADAMTS5*), suggesting that exosome-enriched EVs attenuate the early inflammatory response and thereby limit excessive extracellular matrix degradation.

Previous studies have demonstrated that UCMSC- and ADSC-derived EVs protect cartilage in OA and OCD animal models by suppressing inflammatory signaling and catabolic gene expression (e.g., *MMP13* and *ADAMTS5*), while enhancing anabolic markers such as *COL2* and *ACAN* at later stages (typically 4-8 weeks post-treatment).[38-40] However, there have been limited studies of the early expression dynamics of these genes. In the present study, we demonstrate that combined EV treatment modulates the early inflammatory response, accompanied by a transient downregulation of both catabolic and anabolic gene expression within the cartilage defect microenvironment. This transient suppression of both catabolic and anabolic gene expression in the early phase may reflect a protective regulatory mechanism that dampens excessive inflammatory activation and stabilizes the cartilage microenvironment following injury. During this stage, the local tissue environment is dominated by acute inflammatory signals that can impair cellular anabolic activity and matrix synthesis. Therefore, the observed downregulation of anabolic genes such as COL2 and ACAN may not indicate impaired regeneration but rather a temporary delay in matrix production while the inflammatory milieu resolves.

Beyond suppressing catabolic activity, effective cartilage repair requires promoting anabolic signaling while avoiding premature chondrocyte hypertrophy. *SOX9* serves as a master transcriptional regulator of chondrogenesis by controlling the expression of key cartilage matrix genes such as *COL2*, whereas *RUNX2* and *COL10* are associated with chondrocyte hypertrophy and endochondral ossification.[44,45] Gene expression analyses in the present study indicate that EV treatment favors a regulatory balance characterized by maintained *SOX9*-associated chondrogenic activity alongside the suppression of hypertrophic markers, thereby supporting the preservation of a stable chondrogenic phenotype rather than progression toward terminal differentiation.

Histological and immunohistochemical analyses further supported this mechanistic interpretation. During the early post-injury phase, EV-treated defects exhibited prominent deposition of extracellular matrix components, particularly aggrecan, despite relatively modest cellular proliferation. In contrast, PBS-treated defects exhibited increased cellularity accompanied by localized, heterogeneous matrix accumulation. These findings suggest that exosome therapy may initially promote matrix restoration and microenvironmental stabilization, thereby facilitating subsequent tissue remodeling rather than driving immediate cell-dominant repair. Aggrecan is a critical determinant of cartilage compressive properties and undergoes continuous remodeling under both physiological and pathological conditions.[46] Disruption of aggrecan homeostasis is a hallmark of cartilage degeneration. The distinct spatial and temporal patterns of aggrecan observed following EV treatment suggest that EVs alter the dynamics of ECM remodeling, potentially by limiting early aggrecan degradation while supporting subsequent matrix reorganization toward a more stable reparative phenotype.

The macroscopic, radiographic, and histological evaluations collectively demonstrated progressive repair in both the PBS- and EV-treated groups over the 12-week observation period. However, the EV-treated defects consistently exhibited superior surface integrity, matrix composition, and tissue organization. Notably, the regenerated tissue did not fully recapitulate the native cartilage architecture, indicating that although exosome therapy substantially enhanced repair quality, complete structural regeneration remains challenging.[40]

Taken together, the results support a model in which combined ADSC-EVs and UCMSC-EVs promote cartilage repair primarily through early immunomodulation, suppression of matrix catabolism, stabilization of chondrogenic signaling, and restoration of the extracellular matrix. Rather than inducing rapid cellular proliferation, exosomes appear to reshape the joint microenvironment in a manner that favors sustained and organized tissue regeneration.

Several limitations of the present study should be acknowledged. First, the variation in EV dosing remains a major challenge in defining optimal treatment parameters. Future studies incorporating standardized particle-based normalization and detailed dose-response analyses will be essential to optimizing therapeutic efficacy. Second, this study evaluated a single local injection of combined ADSC-EVs and UCMSC-EVs, which may underestimate the maximal therapeutic potential of repeated dosing, alternative delivery strategies, or scaffold-assisted EV retention. These approaches warrant further investigation.

Third, although gene expression, histological, and macroscopic analyses provided valuable insights into repair dynamics, long-term functional outcomes, particularly the biomechanical performance of the regenerated tissue, were not evaluated. Structural similarities in histological appearance and matrix composition, while encouraging, do not confirm the restoration of the native load-bearing capacity. Future studies should therefore incorporate quantitative biomechanical assessments, such as measurements of the indentation modulus and compressive stiffness, to determine whether EV-mediated repair restores functional integrity comparable to native cartilage, and to evaluate subchondral bone remodeling and defect integration.

Finally, while the combined exosome approach demonstrated beneficial effects, the relative contributions of ADSC-EVs and UCMSC-EVs were not independently assessed. Future mechanistic studies aimed at identifying the specific molecular cargos responsible for immunomodulation and ECM regulation will be critical for optimizing EV-based therapeutic strategies. Moreover, the precise on-target delivery of exosomes to the deeper layers of the injured tissue was not adequately addressed, and the mechanisms underlying the penetration and activity of combined EVs within these regions remain unclear. These limitations highlight important areas for further investigation.

Conclusion

In conclusion, EV-based therapy represents a promising cell-free approach for articular cartilage repair. This study demonstrates that combined EV treatment can attenuate the progression of cartilage defects; however, it does not fully restore tissue properties to those of native cartilage. Continued mechanistic and translational studies are warranted to optimize the EV composition, dosing strategies, and long-term functional outcomes in the context of cartilage regeneration.

Authors' Contribution

Conceptualization: Phuc Van Pham, Ngoc Bich Vu.
Data curation: Phat Thuan Nguyen, Ngoc Bich Vu.
Formal analysis: Phat Thuan Nguyen.
Funding Acquisition: Phat Thuan Nguyen, Ngoc Bich Vu.
Investigation: Phat Thuan Nguyen.
Methodology: Phat Thuan Nguyen, Ngoc Bich Vu.
Project administration: Phuc Van Pham, Ngoc Bich Vu.
Resources: Phuc Van Pham, Ngoc Bich Vu.
Supervision: Phuc Van Pham, Ngoc Bich Vu.
Validation: Phat Thuan Nguyen.
Visualization: Phat Thuan Nguyen.
Writing-Original draft: Phat Thuan Nguyen, Ngoc Bich Vu.
Writing-review & editing: Phat Thuan Nguyen, Phuc Van Pham, Ngoc Bich Vu.

Competing Interests

The authors declare no conflict of interest.

Data Availability Statement

The data supporting the findings of this study are available from the corresponding author upon reasonable request.

Declaration of AI-Assisted Tools in the Writing Procedure

The authors used ChatGPT (OpenAI) and Grammarly to improve the language and clarity of the manuscript. All scientific content, interpretations, and conclusions were developed by the authors, who take full responsibility for the accuracy and integrity of the work.

Ethical Approval

Human umbilical cord tissues used for the isolation of hUCMSCs were obtained from Le Van Thinh Hospital under Sample Supply Contract No. 13/HĐ-BVQ2. Human adipose tissues for hADSC isolation were provided by Emcas Cosmetic Hospital, a licensed tissue banking institution (License No. 15/BYT-GPHĐNHM).

All procedures involving human-derived materials were conducted in accordance with institutional biomedical research ethics regulations and approved by the Institutional Ethics Committee of the Stem Cell Institute, Vietnam National University, Ho Chi Minh City. The cells used in this study were derived from previously approved research projects. Written informed consent was obtained from tissue donors by the hospitals providing the tissue prior to sample collection.

All animal experiments were approved by the Institutional Animal Care and Use Committee (IACUC) of the Stem Cell Institute, Vietnam (Approval No. 230109/SCI-AEC) and were conducted in accordance with relevant national guidelines for the care and use of laboratory animals.

Funding

This research is funded by Vietnam National University, Ho Chi Minh City (VNU-HCM), under grant number CB2025-18-27.

References

1. Dell'Isola A, Recenti F, Giardulli B, Lawford BJ, Kiadaliri A. Osteoarthritis year in review 2025: epidemiology and therapy. *Osteoarthritis Cartilage* **2025**; 33: 1300-6. doi:10.1016/j.joca.2025.08.015
2. Widuchowski W, Widuchowski J, Trzaska T. Articular cartilage defects: study of 25,124 knee arthroscopies. *Knee* **2007**; 14: 177-82. doi:10.1016/j.knee.2007.02.001
3. Johnson-Nurse C, Dandy DJ. Fracture-separation of articular cartilage in the adult knee. *J Bone Joint Surg Br* **1985**; 67: 42-3. doi:10.1302/0301-620x.67b1.3968141
4. Kutaish H, Klopfenstein A, Obeid Adorisio SN, Tscholl PM, Fucentese S. Current trends in the treatment of focal cartilage lesions: a comprehensive review. *EFORT Open Rev* **2025**; 10: 203-12. doi:10.1530/eor-2024-0083
5. Wei W, Dai H. Articular cartilage and osteochondral tissue engineering techniques: recent advances and challenges. *Bioact Mater* **2021**; 6: 4830-55. doi:10.1016/j.bioactmat.2021.05.011
6. Norouzi-Barough L, Shirian S, Gorji A, Sadeghi M. Therapeutic potential of mesenchymal stem cell-derived exosomes as a cell-free therapy approach for the treatment of skin, bone, and cartilage defects. *Connect Tissue Res* **2022**; 63: 83-96. doi:10.1080/03008207.2021.1887855
7. Ng CY, Chai JY, Foo JB, Mohamad Yahaya NH, Yang Y, Ng MH, et al. Potential of exosomes as cell-free therapy in articular

cartilage regeneration: a review. *Int J Nanomedicine* **2021**; 16: 6749-81. doi:10.2147/ijn.S327059

8. Colombo M, Raposo G, Théry C. Biogenesis, secretion, and intercellular interactions of exosomes and other extracellular vesicles. *Annu Rev Cell Dev Biol* **2014**; 30: 255-89. doi:10.1146/annurev-cellbio-101512-122326
9. Lee YJ, Shin KJ, Chae YC. Regulation of cargo selection in exosome biogenesis and its biomedical applications in cancer. *Exp Mol Med* **2024**; 56: 877-89. doi:10.1038/s12276-024-01209-y
10. Ni Z, Zhou S, Li S, Kuang L, Chen H, Luo X, et al. Exosomes: roles and therapeutic potential in osteoarthritis. *Bone Res* **2020**; 8: 25. doi:10.1038/s41413-020-0100-9
11. Wang Y, Kong Y, Du J, Qi L, Liu M, Xie S, et al. Injection of human umbilical cord mesenchymal stem cells exosomes for the treatment of knee osteoarthritis: from preclinical to clinical research. *J Transl Med* **2025**; 23: 641. doi:10.1186/s12967-025-06623-y
12. Hassanpour P, Sadeghsoltani F, Safari MM, Haiaty S, Rahbarghazi R, Mota A, et al. Role of toll-like receptors in exosome biogenesis and angiogenesis capacity. *Bioimpacts* **2025**; 15: 30333. doi:10.34172/bi.30333
13. Cai J, Wu J, Wang J, Li Y, Hu X, Luo S, et al. Extracellular vesicles derived from different sources of mesenchymal stem cells: therapeutic effects and translational potential. *Cell Biosci* **2020**; 10: 69. doi:10.1186/s13578-020-00427-x
14. Hassanzadeh A, Rahman HS, Markov A, Endjun JJ, Zekiy AO, Chartrand MS, et al. Mesenchymal stem/stromal cell-derived exosomes in regenerative medicine and cancer; overview of development, challenges, and opportunities. *Stem Cell Res Ther* **2021**; 12: 297. doi:10.1186/s13287-021-02378-7
15. Zhou Q, Cai Y, Jiang Y, Lin X. Exosomes in osteoarthritis and cartilage injury: advanced development and potential therapeutic strategies. *Int J Biol Sci* **2020**; 16: 1811-20. doi:10.7150/ijbs.41637
16. Mai J, Ke Y, Yao Y. Distinct roles of extracellular vesicles derived from various mesenchymal stem cell sources in bone regeneration: a systematic review and meta-analysis. *Am J Transl Res* **2025**; 17: 5799-813. doi:10.62347/wlnc8175
17. Xie Q, Liu R, Jiang J, Peng J, Yang C, Zhang W, et al. What is the impact of human umbilical cord mesenchymal stem cell transplantation on clinical treatment? *Stem Cell Res Ther* **2020**; 11: 519. doi:10.1186/s13287-020-02011-z
18. Zhou Y, Zhao B, Zhang XL, Lu YJ, Lu ST, Cheng J, et al. Combined topical and systemic administration with human adipose-derived mesenchymal stem cells (hADSC) and hADSC-derived exosomes markedly promoted cutaneous wound healing and regeneration. *Stem Cell Res Ther* **2021**; 12: 257. doi:10.1186/s13287-021-02287-9
19. Trzyna A, Banaś-Ząbczyk A. Adipose-derived stem cells secretome and its potential application in "stem cell-free therapy". *Biomolecules* **2021**; 11: 878. doi:10.3390/biom11060878
20. Théry C, Amigorena S, Raposo G, Clayton A. Isolation and characterization of exosomes from cell culture supernatants and biological fluids. *Curr Protoc Cell Biol* **2006**; 30: 3-22. doi:10.1002/0471143030.cb0322s30
21. Bradford MM. A rapid and sensitive method for the quantitation of microgram quantities of protein utilizing the principle of protein-dye binding. *Anal Biochem* **1976**; 72: 248-54. doi:10.1016/0003-2697(76)90527-3
22. Comfort N, Bloomquist TR, Shephard AP, Petty CR, Cunningham A, Hauptman M, et al. Isolation and characterization of extracellular vesicles in saliva of children with asthma. *Extracell Vesicles Circ Nucl Acids* **2021**; 2: 29-48. doi:10.20517/evcna.2020.09
23. Morales-Kastresana A, Jones JC. Flow cytometric analysis of extracellular vesicles. *Methods Mol Biol* **2017**; 1545: 215-25. doi:10.1007/978-1-4939-6728-5_16
24. Goebel L, Orth P, Müller A, Zurakowski D, Bücker A, Cucchiarini M, et al. Experimental scoring systems for macroscopic articular cartilage repair correlate with the MOCART score assessed by a high-field MRI at 9.4 T--comparative evaluation of five macroscopic scoring systems in a large animal cartilage defect model. *Osteoarthritis Cartilage* **2012**; 20: 1046-55. doi:10.1016/j.joca.2012.05.010
25. Livak KJ, Schmittgen TD. Analysis of relative gene expression data using real-time quantitative PCR and the 2(-ΔΔCT method) method. *Methods* **2001**; 25: 402-8. doi:10.1006/meth.2001.1262
26. Li M, Yin H, Yan Z, Li H, Wu J, Wang Y, et al. The immune microenvironment in cartilage injury and repair. *Acta Biomater.* **2022**; 140: 23–42. doi:10.1016/j.actbio.2021.12.006
27. Xiong M, Zhang Q, Hu W, Zhao C, Lv W, Yi Y, et al. Exosomes from adipose-derived stem cells: the emerging roles and applications in tissue regeneration of plastic and cosmetic surgery. *Front Cell Dev Biol* **2020**; 8: 574223. doi:10.3389/fcell.2020.574223
28. Kim YG, Choi J, Kim K. Mesenchymal stem cell-derived exosomes for effective cartilage tissue repair and treatment of osteoarthritis. *Biotechnol J* **2020**; 15: e2000082. doi:10.1002/biot.202000082
29. Zhao C, Chen JY, Peng WM, Yuan B, Bi Q, Xu YJ. Exosomes from adipose-derived stem cells promote chondrogenesis and suppress inflammation by upregulating miR-145 and miR-221. *Mol Med Rep* **2020**; 21: 1881-9. doi:10.3892/mmr.2020.10982
30. Li P, Lv S, Jiang W, Si L, Liao B, Zhao G, et al. Exosomes derived from umbilical cord mesenchymal stem cells protect cartilage and regulate the polarization of macrophages in osteoarthritis. *Ann Transl Med* **2022**; 10: 976. doi:10.21037/atm-22-3912
31. Wang ZG, He ZY, Liang S, Yang Q, Cheng P, Chen AM. Comprehensive proteomic analysis of exosomes derived from human bone marrow, adipose tissue, and umbilical cord mesenchymal stem cells. *Stem Cell Res Ther* **2020**; 11: 511. doi:10.1186/s13287-020-02032-8
32. Li X, Liu L, Yang J, Yu Y, Chai J, Wang L, et al. Exosome derived from human umbilical cord mesenchymal stem cell mediates miR-181c attenuating burn-induced excessive inflammation. *EBioMedicine* **2016**; 8: 72-82. doi:10.1016/j.ebiom.2016.04.030
33. Zhang S, Chu WC, Lai RC, Lim SK, Hui JH, Toh WS. Exosomes derived from human embryonic mesenchymal stem cells promote osteochondral regeneration. *Osteoarthritis Cartilage* **2016**; 24: 2135-40. doi:10.1016/j.joca.2016.06.022
34. Wang Y, Yu D, Liu Z, Zhou F, Dai J, Wu B, et al. Exosomes from embryonic mesenchymal stem cells alleviate osteoarthritis through balancing synthesis and degradation of cartilage extracellular matrix. *Stem Cell Res Ther* **2017**; 8: 189. doi:10.1186/s13287-017-0632-0
35. Chen Y, Xue K, Zhang X, Zheng Z, Liu K. Exosomes derived from mature chondrocytes facilitate subcutaneous stable ectopic chondrogenesis of cartilage progenitor cells. *Stem Cell Res Ther* **2018**; 9: 318. doi:10.1186/s13287-018-1047-2
36. Shchegolev YY, Sorokin DV, Scherbakov AM, Andreeva OE, Salnikova DI, Mikhaevich EI, et al. Exosomes are involved in the intercellular transfer of rapamycin resistance in the breast cancer cells. *Bioimpacts* **2023**; 13: 313-21. doi:10.34172/bi.2023.27490
37. Khan NZ, Cao T, He J, Ritzel RM, Li Y, Henry RJ, et al. Spinal cord injury alters microRNA and CD81+exosome levels in plasma extracellular nanoparticles with neuroinflammatory potential. *Brain Behav Immun* **2021**; 92: 165-83. doi:10.1016/j.bbi.2020.12.007
38. Zhou H, Shen X, Yan C, Xiong W, Ma Z, Tan Z, et al. Extracellular vesicles derived from human umbilical cord mesenchymal stem cells alleviate osteoarthritis of the knee in mice model by interacting with METTL3 to reduce m6A of NLRP3 in macrophage. *Stem Cell Res Ther* **2022**; 13: 322. doi:10.1186/s13287-022-03005-9
39. Tofiño-Vian M, Guillén MI, Pérez Del Caz MD, Silvestre A, Alcaraz MJ. Microvesicles from human adipose tissue-derived mesenchymal stem cells as a new protective strategy in osteoarthritic chondrocytes. *Cell Physiol Biochem* **2018**; 47: 11-25. doi:10.1159/000489739
40. Woo CH, Kim HK, Jung GY, Jung YJ, Lee KS, Yun YE, et al. Small extracellular vesicles from human adipose-derived stem cells attenuate cartilage degeneration. *J Extracell Vesicles* **2020**; 9: 1735249. doi:10.1080/20013078.2020.1735249
41. Yan L, Wu X. Exosomes produced from 3D cultures of umbilical cord mesenchymal stem cells in a hollow-fiber bioreactor show improved osteochondral regeneration activity. *Cell Biol Toxicol* **2020**; 36: 165-78. doi:10.1007/s10565-019-09504-5
42. Ge XP, Gan YH, Zhang CG, Zhou CY, Ma KT, Meng JH, et al. Requirement of the NF-κB pathway for induction of Wnt-5A by interleukin-1β in condylar chondrocytes of the temporomandibular joint: functional crosstalk between the Wnt-5A and NF-κB signaling pathways. *Osteoarthritis Cartilage* **2011**; 19: 111-7. doi:10.1016/j.joca.2010.10.016

43. Shi S, Man Z, Li W, Sun S, Zhang W. Silencing of Wnt5a prevents interleukin-1β-induced collagen type II degradation in rat chondrocytes. *Exp Ther Med* **2016**; 12: 3161-6. doi:10.3892/etm.2016.3788
44. Wu Z, Korntner SH, Mullen AM, Zeugolis DI. Collagen type II: from biosynthesis to advanced biomaterials for cartilage engineering. *Biomater Biosyst* **2021**; 4: 100030. doi:10.1016/j.bbiosy.2021.100030
45. Chen J, Chen F, Wu X, Bian H, Chen C, Zhang X, et al. DLX5 promotes Col10a1 expression and chondrocyte hypertrophy and is involved in osteoarthritis progression. *Genes Dis* **2023**; 10: 2097-108. doi:10.1016/j.gendis.2022.12.016
46. Plaas AHK, Moran MM, Sandy JD, Hascall VC. Aggrecan and hyaluronan: the infamous cartilage polyelectrolytes - then and now. *Adv Exp Med Biol* **2023**; 1402: 3-29. doi:10.1007/978-3-031-25588-5_1